Author/s:
Benovitski, YB;Lai, A;Saunders, A;McGowan, CC;Burns, O;Nayagam, DAX;Millard, R;Harrison, M;Rathbone, GD;Williams, RA;May, CN;Murphy, M;D'Souza, WJ;Cook, MJ;Williams, CE

Title:
Preclinical safety study of a fully implantable, sub-scalp ring electrode array for long-term EEG recordings

Date:
2022-06-01

Citation:
Benovitski, Y. B., Lai, A., Saunders, A., McGowan, C. C., Burns, O., Nayagam, D. A. X., Millard, R., Harrison, M., Rathbone, G. D., Williams, R. A., May, C. N., Murphy, M., D'Souza, W. J., Cook, M. J. & Williams, C. E. (2022). Preclinical safety study of a fully implantable, sub-scalp ring electrode array for long-term EEG recordings. Journal of Neural Engineering, 19 (3), https://doi.org/10.1088/1741-2552/ac72c1.

Preclinical safety study of a fully implantable, sub-scalp ring electrode array for long-term EEG recordings

Yuri B. Benovitski[1,5], Alan Lai[2], Alexia Saunders[1], Ceara C. McGowan[1], Owen Burns[1], David A.X Nayagam[1,3], Rodney Millard[1], Mark Harrison[1], Graeme D. Rathbone[1], Richard A. Williams[3], Clive N. May[4], Michael Murphy[2], Wendyl J. D'Souza[2], Mark J. Cook[2], Chris E. Williams[1,5]

[1] Bionics Institute, East Melbourne, VIC, Australia
[2] Department of Medicine, The University of Melbourne, St. Vincent's Hospital, Fitzroy, VIC, Australia
[3] Department of Pathology, University of Melbourne, St. Vincent's Hospital, Fitzroy, VIC, Australia
[4] The Florey Institute of Neuroscience and Mental Health, The University of Melbourne, Parkville, VIC, Australia
[5] Medical Bionics Department, University of Melbourne, Parkville, VIC, Australia

Corresponding author: Yuri Benovitski, Bionics Institute, St. Vincent's Hospital, Melbourne, Victoria, Australia. Email address: ybenovitski@bionicsinstitute.org

Abstract

Objective: Long-term electroencephalogram (EEG) recordings can aid diagnosis and management of various neurological conditions such as epilepsy. In this study we characterize the safety and stability of a clinical grade ring electrode arrays by analyzing EEG recordings, fluoroscopy, and computed tomography (CT) imaging with long-term implantation and histopathological tissue response.

Approach: Seven animals were chronically implanted with EEG recording array consisting of four electrode contacts. Recordings were made bilaterally using a bipolar longitudinal montage. The array was connected to a fully implantable micro-processor controlled electronic device with two low-noise differential amplifiers and a transmitter-receiver coil. An external wearable was used to power, communicate with the implant via an inductive coil, and store the data. The sub-scalp electrode arrays were made using medical grade silicone and platinum. The electrode arrays were tunneled in the subgaleal cleavage plane between the periosteum and the overlying dermis. These were implanted for 3-7 months before euthanasia and histopathological assessment. EEG and impedance were recorded throughout the study.

Main results: Impedance measurements remained low throughout the study for 11 of 12 channels over the recording period ranged from 3 to 5 months. There was also a steady amplitude of slow-wave EEG and chewing artifact (noise). The post-mortem CT and histopathology showed the electrodes remained in the subgaleal plane in 6 of 7 sheep. There was minimal inflammation with a thin fibrotic capsule that ranged from 4 to 101µm. There was a variable fibrosis in the subgaleal plane extending from 210 to 3617µm (S3-S7) due to surgical cleavage. One sheep had an inflammatory reaction due to electrode extrusion. The passive electrode array extraction force was around 1N.

Significance: Results show sub-scalp electrode placement was safe and stable for long term implantation. This is advantageous for diagnosis and management of neurological conditions where long-term, EEG monitoring is required.

Keywords

EEG; Electrode; Implant; Impedance; Signal stability; Tissue response

Abbreviations

EEG, Electroencephalogram; CT, Computed tomography; EMG, Electromyography.

1. Introduction

Clinical quality, long-term electroencephalogram (EEG) recordings are crucial for diagnosing multiple neurological conditions such as epilepsy. External recordings are not sufficient in many cases and invasive approaches are common in patients with more complex etiologies. Most of these invasive approaches involve craniotomy and short-term recordings where patients must stay at the hospital. Less invasive devices allow longer-term recordings and less interruption to patients' daily routine. Also, fully implantable, and minimally invasive devices allow recording long-term outside the clinic which is particularly useful during times of quarantine or partial physical isolation.

Commonly used scalp electrodes have a few issues associated with them such as skin abrasion during placement and reduced signal stability due to impedance increase over time (for review see Ferree, Luu et al. 2001). More invasive intracranial arrays require craniotomy thus associated with increased risk and generally used for shorter recording periods (Burneo, Steven et al. 2006). One study tested intracranial arrays long-term showing that impedances are stable over one year (Sillay, Rutecki et al. 2013), however recording quality and the features extracted from the data varied significantly over 100 days following implantation (Ung, Baldassano et al. 2017). Novel endovascular array does not require craniotomy but has relatively narrow spatial resolution (John, Opie et al. 2018). For detailed review of the evolution and acceptance of invasive EEG monitoring techniques see (Reiff, Strzelczyk et al. 2016).

Previously we compared three types of electrodes (disk, ring, and peg) implanted simultaneously (Benovitski, Lai et al. 2017). The results showed that the peg electrode had better signal to noise ratio however the ring was less invasive and able to record adequate EEG. The purpose of this study is to assess the safety and stability of clinical grade ring electrode array with an advanced recording system for translation to trial. Signal stability, impedance, histopathology, anatomical placement, and removability were assessed with long term implantation.

2. Methods

2.1 Subjects

Seven healthy Merino ewes, 1.5-2 years old (S1 to S7) were implanted for an average of 4.9 months range: 3-7 months; standard deviation: 1.7. Sheep were individually housed in 12 h light/dark cycle and given free access to water and fed oaten chaff once a day. Food and water intake and the well-being of the animals were monitored daily. This research was approved by the Florey Institute of Neuroscience and Mental Health Animal Ethics Committee, AEC Number: 18-106-FINMH, that adheres to the Australian code for the care and use of animals for scientific purposes.

2.2 Implant device

A fully implantable, minimally invasive device was developed and tested in house. It consists of titanium encapsulated electronics, a receiver/transmitter coil, and an electrode array. Each array consists of four cylindrical ring electrodes E1-4, with E1-E2 and E3-E4 forming two differential channels. Each channel was connected to a separate differential amplifier housed within a single implantable module (Figure 1). Both amplifiers were coupled to the titanium housing of the module forming a ground for the recording system.

The electrode arrays were fabricated from pure platinum rings and medical grade silicone. The electronics are welded into titanium capsule, which was later fully molded in silicone. All implant components were composed of proven biocompatible materials. Importantly the array was designed to be easily removable.

The first two animals (S1-2) were implanted with a 251mm long array while a shorter 205mm lead was used in later subjects (S3-7) to better match sheep's head size. The spacing between electrode contacts was 50-40-50mm for S1-2 and 35mm for S3-7. In all subjects, array diameter was 1.2mm and the four electrode contacts remained the same (Ø1.2 x 5mm platinum).

2.3 Implant surgery

Surgery was performed under general anesthesia using standard sterile surgery techniques. Anesthesia was induced with intravenous sodium thiopental (15 mg/kg) and following intubation, ongoing anesthesia was maintained with 1.5-2.0% isoflurane/O2. Analgesia was maintained with intramuscular flunixin meglumine (1 mg/kg: Troy Laboratories) at surgery and 4 h post-surgery. Reflexes were tested to ensure adequate anesthesia and vital signs were recorded throughout the procedure. Intramuscular antibiotic (900 mg, procaine penicillin) was administered intraoperatively and 2 days postoperatively.

The placement of the electrode leads, and incisions were marked using a surgical marker and a flexible guide template. After incision and blunt dissection, a custom-made hollow guide cannula was tunneled between the incisions. The cannula tip was removed, and the ring electrode array was inserted into the cannula from one side. Then the cannula was withdrawn from the other side leaving the array between the periosteum and subgaleal plane (Figure 1C). This was repeated on the other side to position the array in a 'U' shape overlying left and right hemispheres (Figure 1D). The fully implantable receiver-transmitter was placed in a subcutaneous pocket in the neck. In Subjects 3 - 7 a reinforced silicone suture patch was used to secure the electrode array to muscle at the nape to minimize implant movement. Subjects 1-3 were also implanted with passive electrode arrays positioned in the subcutaneous area on the left and right dorsal flanks. Impedance was recorded straight after implantation to ensure the functionality of the device, then the incisions were closed.

2.4 EEG recording and processing

EEG was recorded using a battery powered wearable logging data to an SD-card (Figure 1E-G) at 250Hz sampling rate from 12 differential channels in 6 subjects combined. Data from subjects 1 to 6 were used for this purpose. The last animal was excluded from EEG analysis as a different version of the implant and wearable electronics were used. About 40 hours of EEG data were recorded every week for each animal. This was the wearable battery life for one recording session. Recordings were made after 1-3 weeks of recovery after implantation surgery and a week before termination. While the implantation periods were between 3 to 7 months, the recording periods were shorter and ranged from 3 to 5 months. All signals were calibrated, and timing of events were synchronized.

EEG data was categorized into the following segments: chewing, slow-wave, simultaneous chewing and slow-wave, other electromyography (EMG), and baseline. Chewing is a distinct case of EMG where signal goes back to normal between jaw clenches. For representative examples of the different data segments see Figure 2. Labeling was done by observing 10 second windows of raw signal, spectrogram (0 to 128Hz range), and longer window (10 minute) amplitude EEG (aEEG). An accelerometer (Analog Devices, ADXL335 - 3-Axis ±3 g, red arrow in Figure 1G) inside the wearable that was attached to the back of the animal and used to select segments of EEG data during which the animal was not moving. This was done by visually confirming that the accelerometer output was stable. Accelerometer data was used to determine that animal's body was stationary however it could still be chewing which was presented as an EEG artifact. Overall, 327, 507, 637, 1739, 1680, and 296 segments were marked for subjects 1 to 6, respectively.

All segments were processed into two different frequency ranges (similar to Benovitski, Lai et al. 2017): the EEG band below 30Hz cut-off and above 30Hz for higher (non-EEG) frequency components. This is a way of measuring signal to noise ratio as below 30Hz is highly relevant to detect epileptiform spike activity and above 30Hz EEG is more impacted by noise such as EMG. The high-pass and low-pass filters were Butterworth, 3rd order with stop-band attenuation of 60dB. The peak-to-peak amplitude for each frequency band and the ratio between EEG band and high frequency were calculated. Signal to noise ratio was defined as chewing artifact index which is the ratio between the two amplitudes for the segments with simultaneous chewing and slow wave EEG (Figure 3). Left-right channel cross-coherence (cross-correlation in frequency domain) was calculated for each data segment type over the study period. This was achieved by measuring cross-coherence function amplitude between the left and right channels. Data were analyzed across all 24 electrodes and presented as median (upper and lower quartile) for each electrode type. Matlab version R2021a (MathWorks Inc., MA, USA) and LabVIEW version 18 (National Instruments Corp., Texas, USA) were used for data labeling, filtering, and post-processing.

2.5 Impedance approximation

Continuous impedance measurements of the tissue-electrode contact were made throughout the chronic implantation period. This impedance measurements were conducted at a single frequency (62.5Hz) and low-amplitude bi-phasic pulse with a linear response between 100Ω and 34kΩ. This was calibrated to a switchable resistor and fixed capacitor model. A bi-phasic current pulse was used instead of a sinusoidal current source due to implanted electronics module space constraints. This is a simplified impedance measurement and conducted continuously every 10 minutes and averaged over 10-hour periods (Figure 3B) throughout the study.

A full impedance spectroscopy on the separate, passive 14 individual electrodes were conducted after the animals were euthanized and prior histological preparation. Measurements were made using Z100 - Interface 1000 potentiostat (Gamry Instruments) with adjacent electrode as reference and the other

channel (2 electrodes) as counter using. Values at 60Hz were considered as this was close to the 62.5Hz used to measure the simplified and continuous impedance.

Measuring impedance at 62.5 Hz is not an industry standard (normally 1000 Hz) thus only an approximation. This frequency was selected due to the reduced sampling rate of the implant and outside the useful range for EEG measurements. It was measured periodically thus still provides useful information regards electrodes' long-term state.

2.6 Imaging

Fluoroscopy imaging was conducted intra-operatively and tissue harvested after 3-7 months of implantation were scanned with computed tomography (CT, Siemens Somatom). The CT images were used to assess overall lead placement and guide trimming of the samples to the electrode position for histological processing.

2.7 Histopathology

After animals were euthanized, skull and scalp tissue were fixed, and the samples were decalcified. Electrodes were localized in quadrants from the CT images and lines were drawn across the tissue, intercepting the lead and ring electrodes. An incision through the scalp to the bone severed the lead. The lead and rings were then removed, and the ring electrode location identified with tissue dye. The quadrants were dissected, and ring electrode pockets were visible. These samples were then paraffin embedded, sectioned, hematoxylin and eosin stained.

Distance of electrode cavity to skull (Figure 5), fibrotic encapsulation (Figure 6), fibrosis due to tunneling (Figure 7), and peri-implant fibrosis (Figure 8) were measured for subjects S3-7. The first two subjects histological preparations were used for method development. Fibrotic encapsulation was measured in 4 equidistant locations at the superior, inferior, and left and right margins. Distance from implant cavity to skull was measured from the inferior implant pocket to skull. A clinical pathologist (RW) assessed the tissue surrounding the ring cavities for immunological and tissue response for subjects S3-7 (Table 1).

Some measurements may be exaggerated by more oblique sectioning of the region. This also could be the reason why cavities appear elongated. However, some artefacts due to the processing (e.g., fixing the tissue) and removal of the electrode array are also possible.

2.8 Passive array removability

The main electrodes couldn't be extracted as they needed to remain in place for tissue fixation and histopathological analysis, thus extra four passive electrode arrays were implanted in the left and right dorsal flanks of subjects S1-3 and were extracted during termination post chronic implantation. The proximal end of the array was located by palpation of the skin then exposed via a skin incision. A Mark-10 strain gauge was attached to the array and extraction force was measured over time while manually pulling the array out.

3. Results

Fluoroscopy, CT, EEG, impedance, and histopathology from 24 electrodes (12 differential channels) were assessed across 7 subjects. Post-mortem CT scans indicate that the position of the electrode arrays was variable across subjects. All except one (23 of 24) electrode remained in the subgaleal plane in 6 of 7 sheep.

Differential channel recordings (Figure 2 and 3) were made during the implantation period. Figure 4 shows the three signal stability metrics for all subjects over the recording period. The metrics include simplified impedance (A), chewing artifact index (B), and left-right channel cross-coherence (C). All three different metrics remained steady over 3-5 months. After tissue assessment of one of the subjects there was evidence of array erosion through the scalp probably due to a twist in the lead, this lesion was associated with doubling of impedance (S2 Ch2, 3rd month, inset A). S03 had higher chewing artifact index (inset B), probably due to better superior placement over cerebral hemispheres. S1 had higher left-right channel correlation (inset C) but only two months of recordings due to problems with keeping the wearable on the animal.

Out of 16 electrodes that could be assessed using high enough quality axial CT images, all electrode contacts were positioned on the correct side. However, 2 of 16 ended up adjacent to midline and 1 of 16 too far from midline. Based on histological analysis, median distance of the ring cavity to skull was 941 ranging from 409 to 5028µm (S3-7).

Histopathology showed that the electrodes were encapsulated within a thin fibrotic capsule. Fibrotic tissue extended vertically from either side of the cavity due to the intraoperative cleavage opening (electrode insertion procedure). Overlying the electrode cavity was a loose connective layer and scalp. One sheep had an inflammatory reaction with electrode extrusion. There were three examples of twists or looping of the lead and in 3 examples the tip was curled back. For representative images of the ring electrode array in tissue and cavities after processing for histopathological assessment see Figure 5. Fibrotic encapsulation measurements and representative example are shown in Figure 6. Summary of the subgaleal cleavage plane measurements and photomicrograph examples adjacent to the ring cavity are shown in Figure 7. Peri-implant fibrosis measurements for S3-7 and examples are shown in Figure 8.

Immunological response of tissue surrounding the implant was scored by a clinical pathologist (RW) for; histiocytic response, chronic mononuclear inflammatory response, acute inflammation (caused by infection), in addition to bone and periosteum response. The scoring showed a variation in tissue response within and across subjects (Table 1). The histiocytic response varied, ranging from not present up to multilayered with multi nucleated giant cells. Each of the subjects (S3-7) observed displayed minimal chronic inflammation with S7 exhibiting a higher response. A low level of acute inflammation was observed with S7 displaying an increased response. Bone appeared normal is S2-5 and S7, however S6 may reflect a pathological change to the bone. Periosteum morphology appeared normal.

The passive electrode array was pulled out without breaking, extraction force was measured at around 1N, see representative example in Figure 9.

Full impedance spectroscopy on the separate, passive electrode arrays median was 0.8kΩ (0.7 lower and 1.2 upper quartiles, n=14). While the two measurements are technically different, the values were comparable with the continues simplified impedance measurement median of 0.69kΩ. A representative example of impedance spectroscopy of the passive electrodes after termination is shown in Figure 10.

4. Discussion

This study demonstrates consistent long-term EEG and impedance recordings using a two-channel ring electrode array in sheep. This approach allows minimally invasive implantation and relatively easy removal compared to other types of electrodes. These may be useful for specific diagnostic and monitoring for epilepsy and other indications that rely on recordings.

4.1 Surgical approach

Ring electrode arrays tunneled under the scalp, enable minimally invasive surgical techniques to be used for implantation and removal. The electrode array was permanently attached to the electronics package.

A combination of blunt dissection and a guide cannula was used to create a tissue pocket and allowed for subgaleal electrode placement. Reducing the need for a blunt dissection and relying more on custom cannula insertion tool would result in smaller cleavage plane with less fibrosis, and therefore be a less traumatic implantation.

Ideal electrode placement was not possible in all subjects with twists and curled tips in 3 animals. However, electrode contacts for left and right channels remained on the correct side of the brain. From axial CT images, 2 of 16 electrode contacts ended up adjacent to midline and 1 of 16 was positioned too far from midline. In these 3 cases the other electrode for the same channel was in good position so EEG could still be recorded.

In one animal (S2) we positioned the receiver-transmitter on the head. Due to relatively small sheep head size, this resulted in the tip electrode sitting over the implant body (transmitter) and may have caused erosion through the scalp, we do not expect this to be an issue in humans as the head is larger.

4.2 Signal stability

Signal stability was assessed by impedance, chewing artifact index, and left-right channel cross-coherence. The low impedance and chewing artifact index (slow wave EEG and chewing artifact amplitude ratio) remained steady throughout the recording period (3-5 months) meaning that long-term EEG recording could be achieved. This was despite some variability in anatomical placement of the electrode arrays. One study reported long-term impedance measurements from 188 patients to be 0.57 and 0.9kΩ for depth and subdural leads, respectively (Sillay, Rutecki et al. 2013). While electrodes were made from different material (platinum-iridium alloy vs. pure platinum) and surface area (7.9 vs. 50 mm^2), the sub-scalp measurements from the current study were similar (0.69kΩ).

The example of increased impedance with erosion suggests that regular monitoring of impedance in future subjects could improve discovery of adverse events such as erosion in a timely fashion. Overall, the consistently low impedance and electrophysiologic measures relate to the minimal pathological response and stable placement under the scalp.

The electrode spacing was configured for recording of spatially summed EEG potentials from pairs of electrodes over the left and right hemispheres. There was some variability in placement due to the constraints of the small sheep skull and relatively large temporalis muscles.

EEG recordings were made bilaterally using a bipolar longitudinal montage (both hemispheres), this is the minimum number of channels used in channel reduction studies and important for specific left and right sided diagnosis of neurological conditions. One of these studies showed that adding two mirrored channels provided high performance and negligible increase in performance when adding more channels.

More importantly, these studies show that computational cost increases significantly with addition of extra electrodes which can be a determining factor when designing a fully implantable system with on-board signal processing (Faul and Marnane 2012, Alotaiby, Abd El-Samie et al. 2015).

4.3 Histopathology

Subjects S3-7 underwent full histological assessment. Minimal fibrotic encapsulation was observed in tissue surrounding the implant cavity, this was anticipated given the implant was made of biocompatible materials. There was minimal fibrous scarring beside the implant, along the plane of surgical dissection.

The length of fibrosis extending laterally from the electrode cavity along the subgaleal cleavage plane was variable. This was due to different levels of blunt dissection used during implantation. The fibrotic response in this area was minimal and it did not impact any of the signal stability metrics. However, optimizing a tunneling tool to minimize the need for blunt dissection could reduce the extent of surgical trauma in future studies.

Overall, histopathology after long-term implantation suggest that the ring electrode can be safely implanted for up to 7 months.

4.4 Removability

At the end of the study, the passive electrode arrays were pulled out while measuring extraction force. The array removal forces were around 1N, as extraction forces in the subgaleal space are expected to be higher, the lead was designed to withstand removal forces up to 10-15N. In another study, electrodes were pulled out of muscular tissue with a range of forces dependent on the period of implantation, the rate of increase in the peak force was most rapid during the first week (Bhadra and Mortimer 2006).

There were some cases of twists in the lead which may impede removal. However, the minimal fibrosis, consistent diameter of the lead, and low removal force suggest potential ease of removal following long-term implantation.

4.5 Study limitations

The sheep anatomy has limitations including small skull size and large temporalis muscles relative to humans. This constrained placement to the U configuration and caused increased chewing artifacts amplitude relative to the EEG. The other limitation was a difficulty positioning all the electrodes superior to the cerebral hemispheres. This, however, did not seem to impede EEG signal stability, this was probably to do with the fact that recordings were made differentially from pairs of electrodes thus individual differences in placement had minimal influence.

Animal subjects in the current study didn't have epilepsy thus no epileptiform spike activity could be recorded, a clinical version of this device is currently being tested in humans with epilepsy.

This study was mainly conducted to establish histopathological safety thus subjects had to be sacrificed for tissue sample collection, follow up after electrode removal was not possible.

The passive electrode removal force was measured with the electrode in the soft tissues of the flank. Given that the active electrodes were implanted subgaleally and the galea and skull have different tissue properties than axial soft tissues, bone erosion and different levels of encapsulation could result in substantial differences in extraction force.

It was not possible to confirm that animals had no sequelae after removal of the device, histopathological scoring is used as indication of potential issues. A full removability study is planned in human subjects,

one human subject was already explanted and no adverse reaction during and post explanation was observed (unpublished).

Standard human EEG for epilepsy, 10/20 montage has 19 electrodes placed in a specific fashion. For an implantable system, the number of electrodes has to be reduced so that it can be implanted with minimal impact. Electrode reduction studies suggest that a useful seizure detection and prediction can be achieved with two to three channels (Salant, Gath et al. 1998, Truong, Kuhlmann et al. 2017). Another successful two channel (3 electrode) study was recently conducted (Viana, Remvig et al. 2021), while also 2-channel, the novelty of the current device is 4 electrodes implanted bilaterally over left and right hemispheres. A clinical version of the current implant is being validated, preliminary results suggest reasonable correlation between the standard 10-20 video EEG and the two-channel sub-scalp recordings (Stirling, Maturana et al. 2021).

Accelerometer motion was validated by visual inspection. As it was placed on the back of the animal, body movement resulted in a high change (sensitivity) while head and jaw (chewing) motion were almost not detectable. In future studies we plan continuous video recording to better define threshold and validate accelerometer data further.

4.6 Conclusion

Together the pathology, electrophysiology, and impedance results indicate that sub-scalp placement can be safe and stable for long term implantation. The minimal fibrotic capsule and low removal forces are consistent with ease of removal. This can yield low tissue-electrode impedance and consistent EEG quality suitable for clinically relevant, chronic recordings. This can be advantageous for diagnosis and management of epilepsy, stroke, sleep, dementias, and other neurological conditions.

Declaration of interest

MM, WD, MC, and OB have a financial interest in the EEG device company EpiMinder. Other authors declare no potential conflicts of interest with respect to the research, authorship, and/or publication of this article. All authors confirm reading the journal's position on issues involved in ethical publication and affirm that this report is consistent with those guidelines.

Funding

The authors acknowledge the current financial support from Epiminder Pty Ltd, and earlier support from the Australian National Health and Medical Research Council Project Grant (APP1075347), and Thyne Reid Foundation (Perpetual financial services). The Bionics Institute acknowledges the support it receives from the Victorian Government through its Operational Infrastructure Support Program.

The funding sources had no involvement in study design, collection, analysis and interpretation of data, writing of the report, or the decision to submit the article for publication.

Author contributions

Conception and study design: CW, MC, GR, WD

Histology: CCM, AS, DN, RW

Electrical, mechanical, and software design: RM, OB, YB, MH

Surgery: CNM, MM, AS

Data collection and analysis: CCM, AS, YB, AL, CW

Writing and analysis: All authors

Acknowledgements

The authors thank Tony Dornom, Tom Vale from the Florey Institute for providing animal care and help with surgeries. Authors would also like to thank Monash Biomedical Imaging and St. Vincent's Institute for help with CT imaging and St. Vincent's Anatomical Pathology for help with histopathology. We thank all reviewers for volunteering their time and providing invaluable feedback.

References

Alotaiby, T., F. E. Abd El-Samie, S. A. Alshebeili and I. Ahmad (2015). "A review of channel selection algorithms for EEG signal processing." EURASIP Journal on Advances in Signal Processing **2015**(1): 1-21.

Benovitski, Y. B., A. Lai, C. C. McGowan, O. Burns, V. Maxim, D. A. X. Nayagam, R. Millard, G. D. Rathbone, M. A. le Chevoir, R. A. Williams, D. B. Grayden, C. N. May, M. Murphy, W. J. D'Souza, M. J. Cook and C. E. Williams (2017). "Ring and peg electrodes for minimally-Invasive and long-term sub-scalp EEG recordings." Epilepsy Res **135**: 29-37.

Bhadra, N. and J. T. Mortimer (2006). "Extraction force and tissue change during removal of a tined intramuscular electrode from rat gastrocnemius." Annals of biomedical engineering **34**(6): 1042-1050.

Burneo, J. G., D. A. Steven, R. S. McLachlan and A. G. Parrent (2006). "Morbidity associated with the use of intracranial electrodes for epilepsy surgery." Canadian journal of neurological sciences **33**(2): 223-227.

Faul, S. and W. Marnane (2012). "Dynamic, location-based channel selection for power consumption reduction in EEG analysis." Computer methods and programs in biomedicine **108**(3): 1206-1215.

Ferree, T. C., P. Luu, G. S. Russell and D. M. Tucker (2001). "Scalp electrode impedance, infection risk, and EEG data quality." Clin Neurophysiol **112**(3): 536-544.

John, S. E., N. L. Opie, Y. T. Wong, G. S. Rind, S. M. Ronayne, G. Gerboni, S. H. Bauquier, T. J. O'Brien, C. N. May, D. B. Grayden and T. J. Oxley (2018). "Signal quality of simultaneously recorded endovascular, subdural and epidural signals are comparable." Sci Rep **8**(1): 8427.

Reiff, P. S., A. Strzelczyk and F. Rosenow (2016). "The history of invasive EEG evaluation in epilepsy patients." Seizure-European Journal of Epilepsy **41**: 191-195.

Salant, Y., I. Gath and O. Henriksen (1998). "Prediction of epileptic seizures from two-channel EEG." Med Biol Eng Comput **36**(5): 549-556.

Sillay, K. A., P. Rutecki, K. Cicora, G. Worrell, J. Drazkowski, J. J. Shih, A. D. Sharan, M. J. Morrell, J. Williams and B. Wingeier (2013). "Long-term measurement of impedance in chronically implanted depth and subdural electrodes during responsive neurostimulation in humans." Brain stimulation **6**(5): 718-726.

Stirling, R. E., M. I. Maturana, P. J. Karoly, E. S. Nurse, K. McCutcheon, D. B. Grayden, S. G. Ringo, J. M. Heasman, R. J. Hoare, A. Lai, W. D'Souza, U. Seneviratne, L. Seiderer, K. J. McLean, K. J. Bulluss, M. Murphy, B. H. Brinkmann, M. P. Richardson, D. R. Freestone and M. J. Cook (2021). "Seizure Forecasting Using a Novel Sub-Scalp Ultra-Long Term EEG Monitoring System." Front Neurol **12**: 713794.

Truong, N. D., L. Kuhlmann, M. R. Bonyadi, J. W. Yang, A. Faulks and O. Kavehei (2017). "Supervised learning in automatic channel selection for epileptic seizure detection." Expert Systems with Applications **86**: 199-207.

Ung, H. M., S. N. Baldassano, H. Bink, A. M. Krieger, S. Williams, F. Vitale, C. Y. Wu, D. Freestone, E. Nurse, K. Leyde, K. A. Davis, M. Cook and B. Litt (2017). "Intracranial EEG fluctuates over months after implanting electrodes in human brain." Journal of Neural Engineering **14**(5).

Viana, P. F., L. S. Remvig, J. Duun-Henriksen, M. Glasstetter, M. Dumpelmann, E. S. Nurse, I. P. Martins, A. Schulze-Bonhage, D. R. Freestone, B. H. Brinkmann, T. W. Kjaer and M. P. Richardson (2021). "Signal quality and power spectrum analysis of remote ultra long-term subcutaneous EEG." Epilepsia **62**(8): 1820-1828.

Figures and Tables

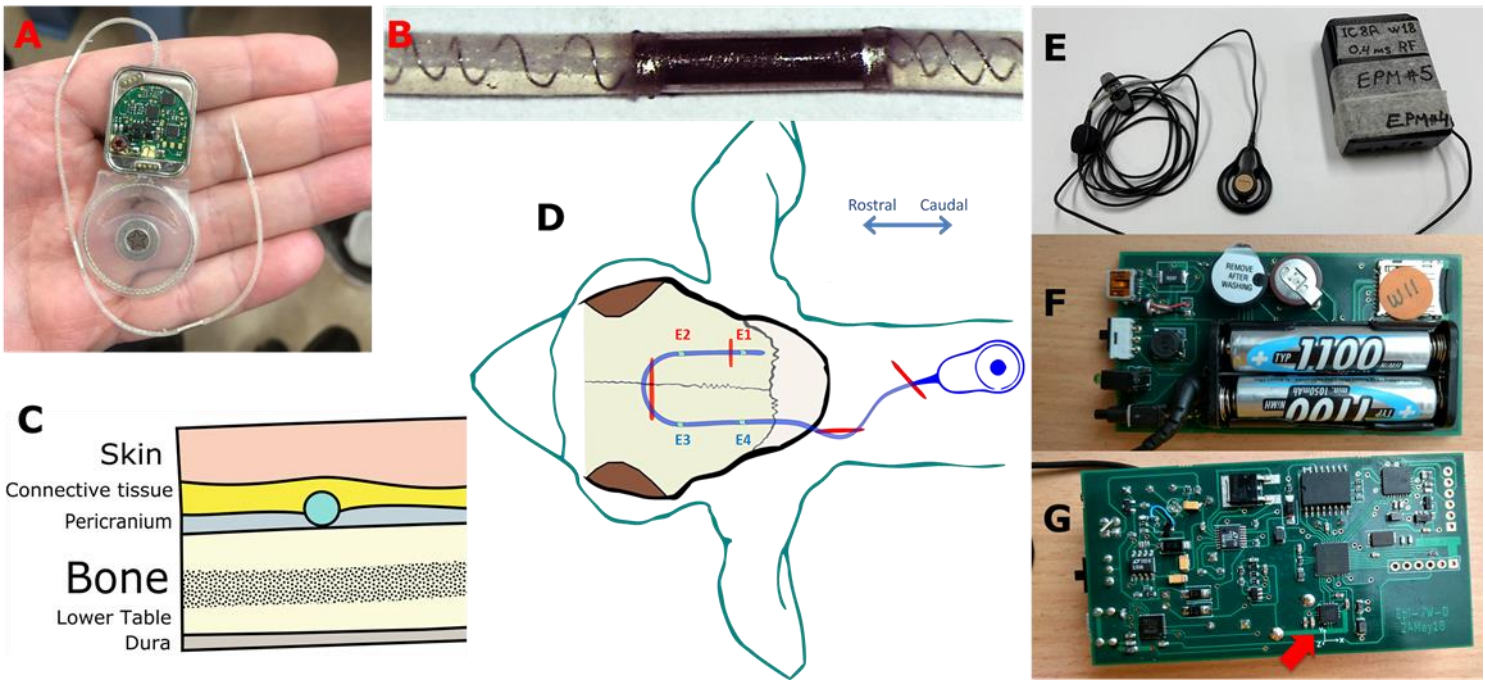

Figure 1 Whole system design includes a (A) custom implant with two analog differential recording channels (amplifiers, INA333, Texas Instruments, gain=1000, bandwidth=350Hz, CMRR=100dB), (B) electrode array with all electrode contacts dimension of Ø1.2 x 5mm made from platinum, (C) anatomical target placement of the whole implant in sagittal and (D) coronal planes with left (blue) and right (red) channels electrode positions (E1, E2, E3, E4) are labeled and surgical incision sites marked by red lines. (E) wearable and coil RF link (F) top electronics with 2x1050mAh NiMH batteries and SD-card and (G) bottom electronics with accelerometer location indicated by red arrow.

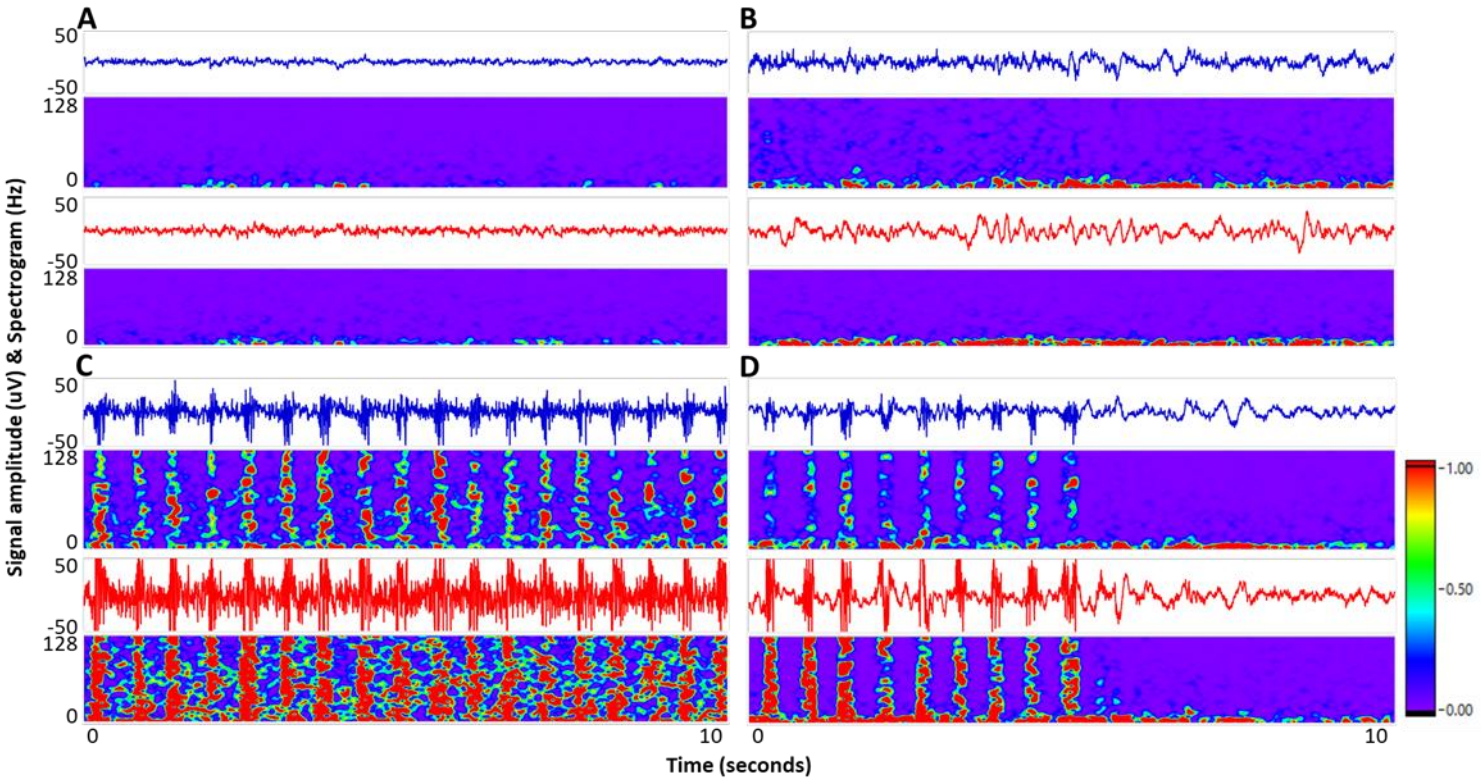

Figure 2 Representative examples of (A) Baseline, (B) slow-wave, (C) chewing, (D) chewing and slow-wave; S5 left (blue) and right (red) channel over 10sec, night-time with stable accelerometer (flatlined), raw signal window +/-50uV, spectrogram range is 0-128Hz. Chewing was collected after feeding while

baseline, slow-wave, and combined chewing (rumination) and slow-wave were collected during nighttime. All spectrograms are Hanning window in steps of 2 samples, 64 window length, and 512 frequency bins.

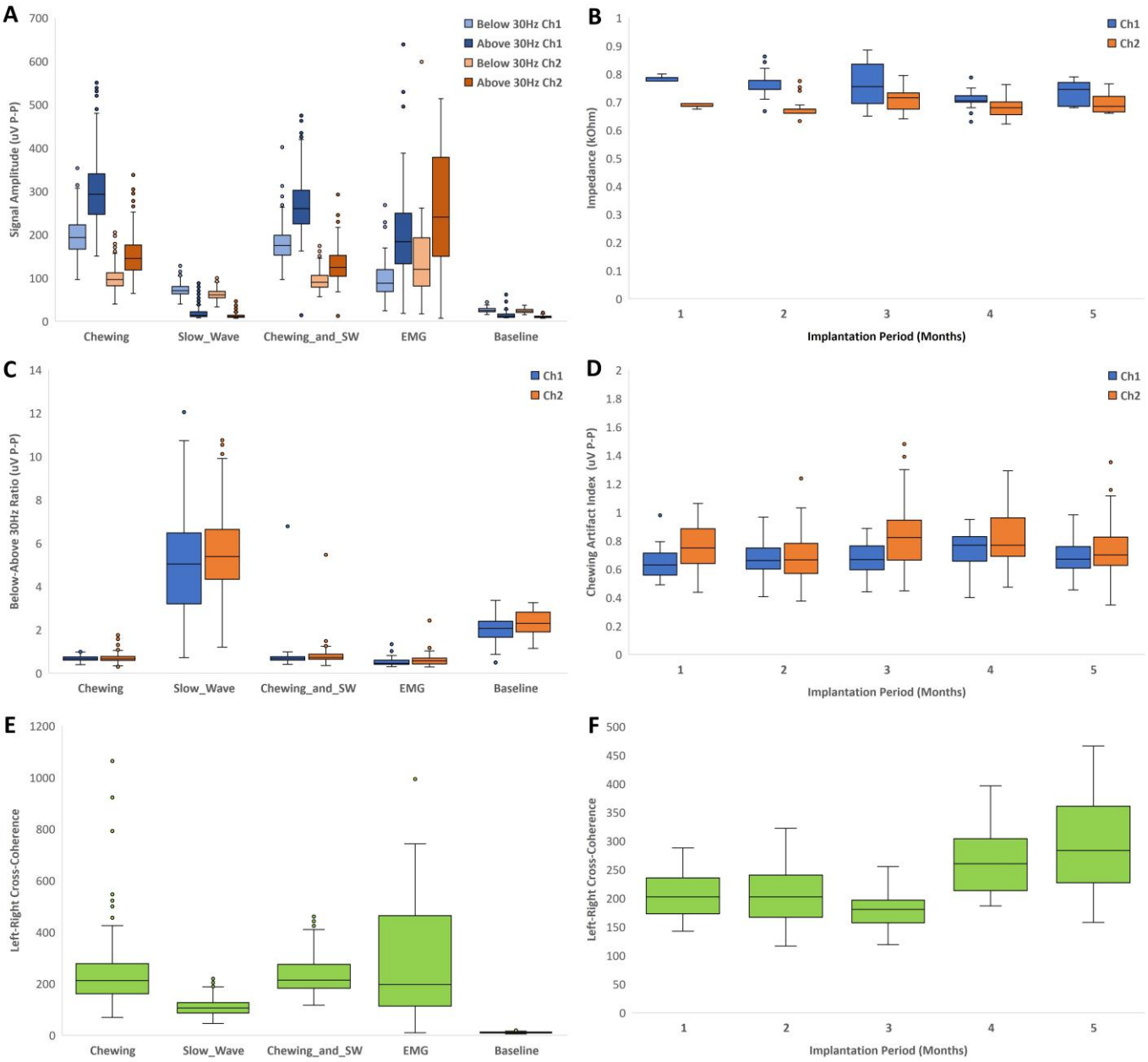

Figure 3 Representative examples (S04) of (A) signal amplitude below and above 30Hz for each segment type, (B) median simplified impedance over the recording period of 5 months, (C) below and above 30Hz ratio for different segment types which is higher for slow-wave and lower for chewing segments as expected, (D) chewing artifact index defined as below-above 30Hz ratio for simultaneous chewing and slow-wave over 5 months, (E) left-right channel correlation (cross-coherence function amplitude) for different segment types, and (F) over 5 months for simultaneous chewing and slow-wave. All insets show medians, outliers, and whiskers that represent upper and lower quartiles. (C) chewing artifact index defined as below-above 30Hz ratio for simultaneous chewing and slow-wave over 5 months (D), left-right channel correlation (cross-coherence function amplitude) for different segment types (E), and over 5 months for simultaneous chewing and slow-wave (F). All insets show medians, outliers, and whiskers that represent upper and lower quartiles. Left insets are between segment types while right insets are over

time. Measurements over period of 5 months is shown for every month. Overall, 1739 epochs of 10 second were labeled for S04 (556 chewing, 833 slow-wave, 285 simultaneous chewing and slow-wave, 33 EMG, and 32 baseline).

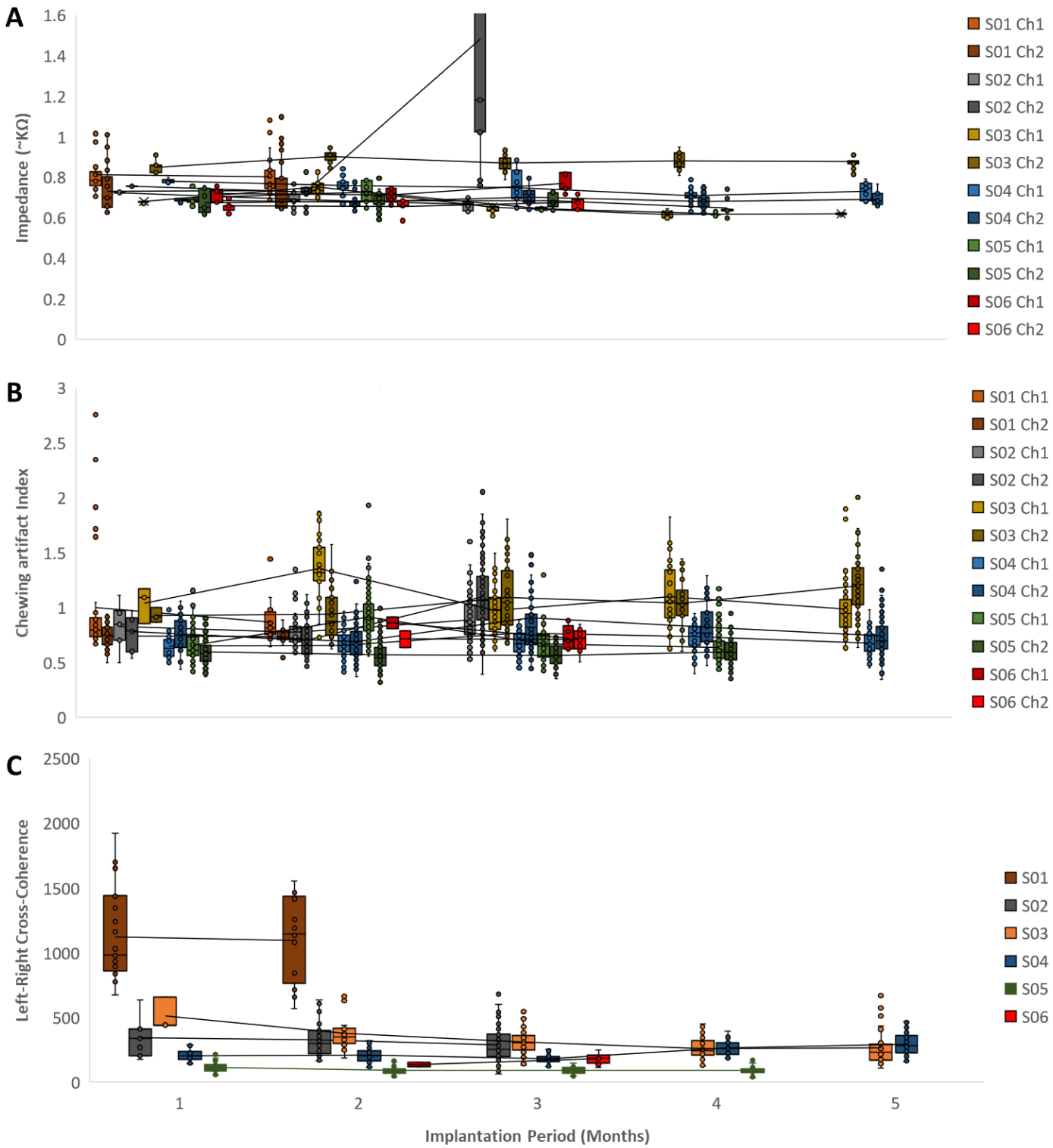

Figure 4 Signal quality measures for 6 subjects (S1-6) over time; (A) simplified impedance, (B) Chewing artifact index, and (C) left-right channel cross-coherence function amplitude. All three different metrics remained steady as shown by the black lines connecting the means over 3-5 months of recording. S02 had increased impedance measured on one of the channels (S02, Ch2, inset A). S03 had higher chewing artifact index (inset B). S1 had higher left-right channel correlation (inset C). All insets show median and upper and lower quartiles. Some data is missing as recordings from different subjects were made for different periods (between 3 to 5 months). In all charts, lines connecting the means, inner and outlier points are shown.

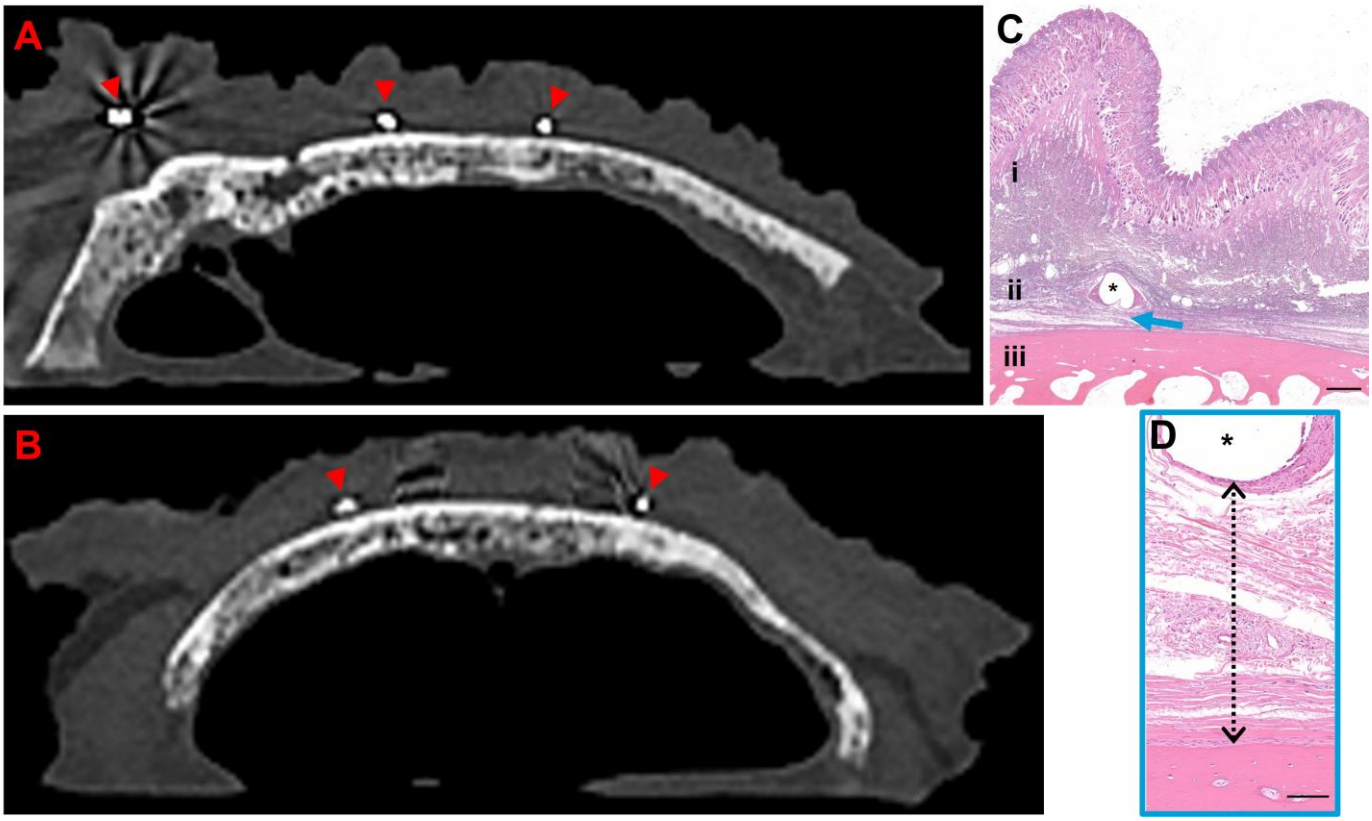

Figure 5 Ring electrode array in tissue and cavities after processing for histopathological assessment. Insets A and B are example CT of a skull and scalp sample with sections of the implanted ring electrode array, marked with triangle arrows, in sagittal and coronal planes, respectively. Inset C (scale bar = 1mm) shows a photomicrograph of hematoxylin and eosin stained, 5 µm thick paraffin embedded tissue section illustrating the histology surrounding the ring electrode cavity (*) with subcutaneous tissue (i), subgaleal tissue (ii), the skull (iii), and arrow indicating high magnification section in inset D. Inset D (scale bar = 100µm) shows the area between the electrode cavity and the skull. The distance from the cavity to the skull (dashed arrow) was measured from the inner lining of the fibrotic encapsulation to the surface of the skull, and measurements of artefactual tearing was subtracted. The skull and periosteum were unremarkable.

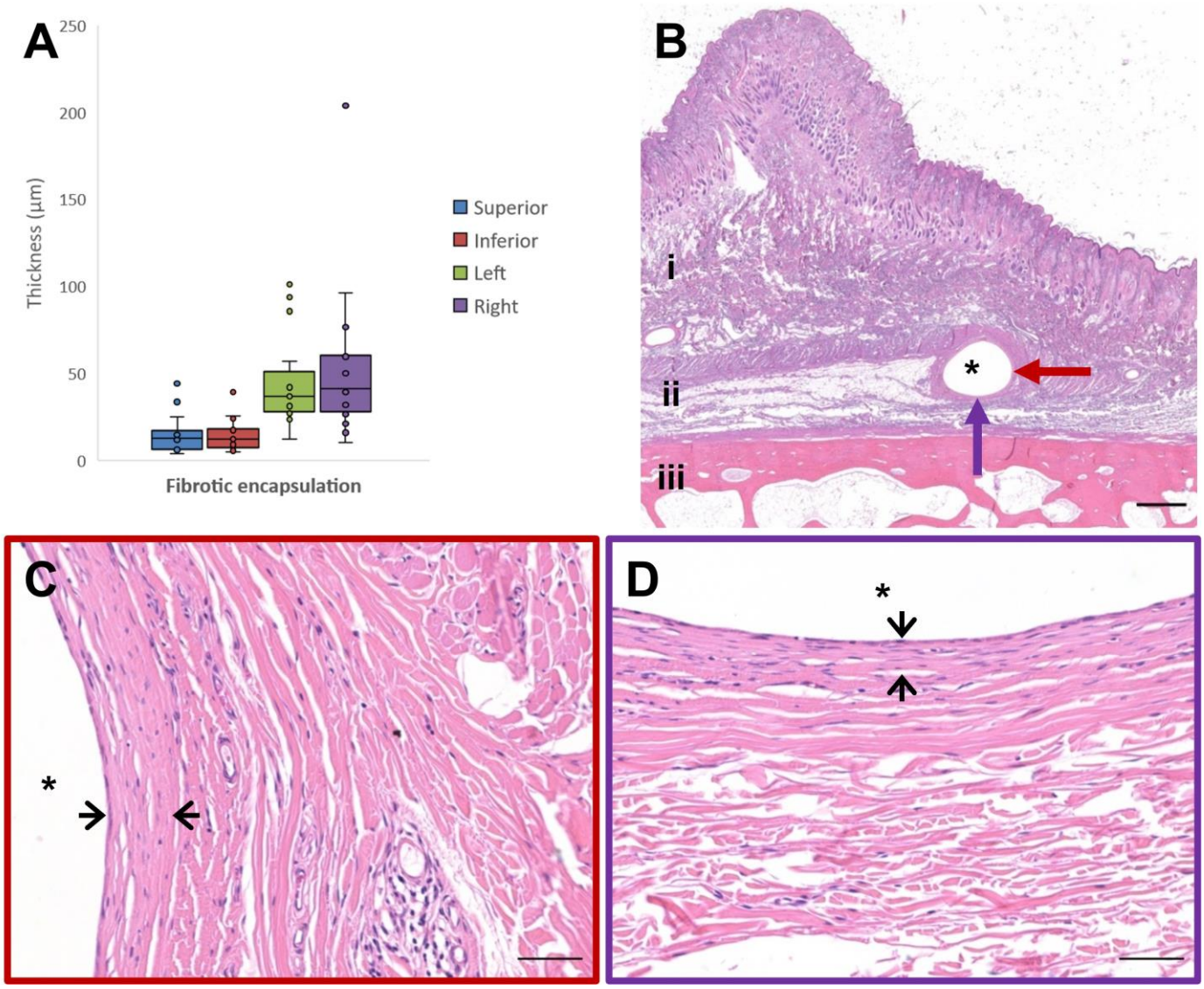

Figure 6 Fibrotic encapsulation measurements and example. Inset A is a summary of all fibrotic encapsulation thickness measured around the ring cavity for 20 samples collected from S3-7. Inset B (scale bar = 1mm) is a photomicrograph of hematoxylin and eosin stained, 5 µm thick paraffin embedded tissue section illustrating the histology surrounding the ring electrode cavity (*) with subcutaneous tissue (i), subgaleal tissue (ii), the skull (iii) and arrows indicating high magnification sections in insets C and D (scale bar = 50µm). Thickness of fibrotic encapsulation were measured (open arrows) on the left (e.g., inset C), right, superior, and inferior (e.g., inset D) sides of all cavities. Overall, fibrotic encapsulation surrounding the ring electrode cavity and tissue inflammatory response was minimal. Histiocytes were observed within the thin fibrotic capsule (not depicted in photomicrograph). The skull and periosteum were unremarkable.

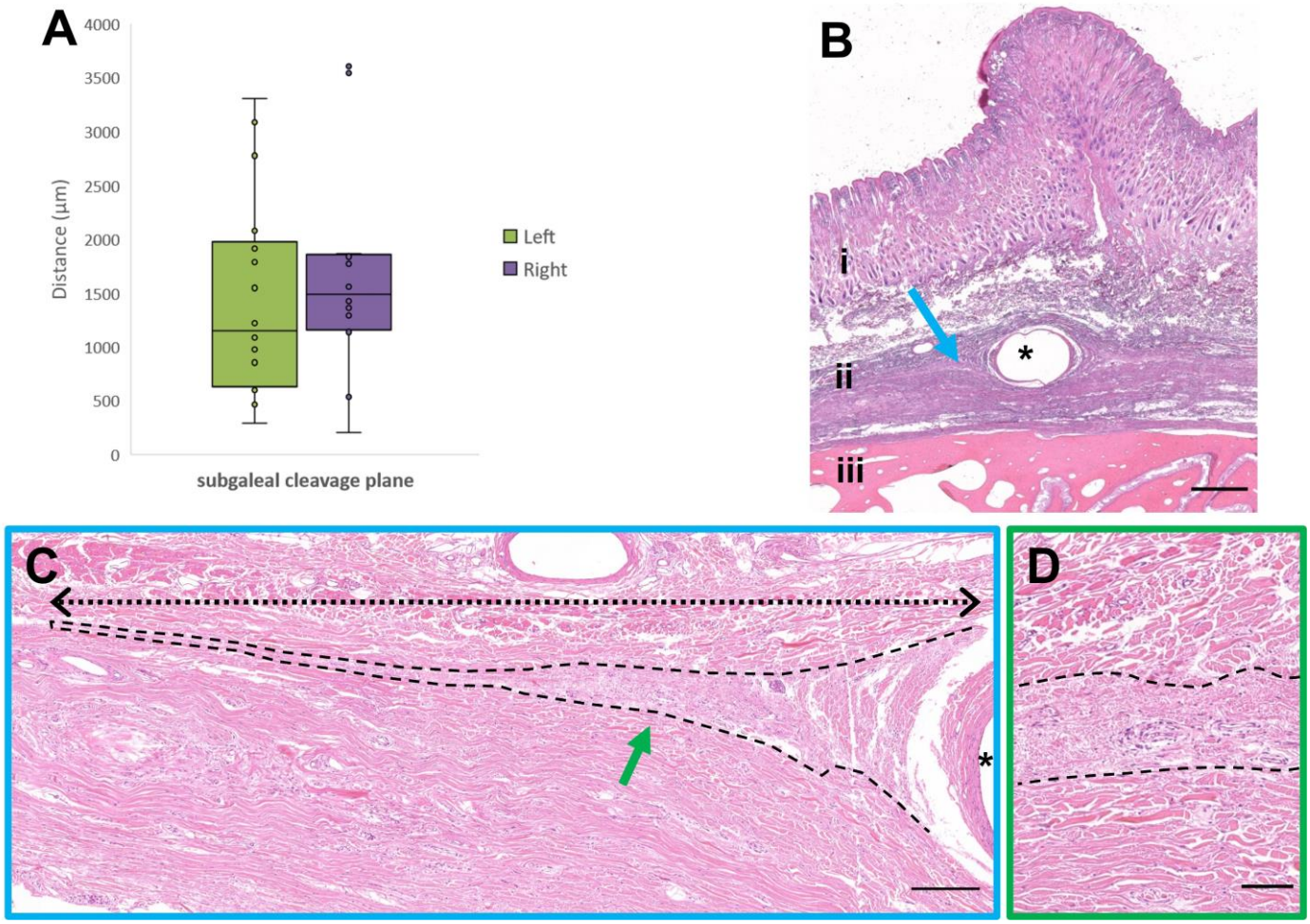

Figure 7 Inset A is a summary of all subgaleal cleavage plane measurements adjacent to the ring cavity for 20 samples collected from S3-7. Inset B (scale bar = 1mm) is a photomicrograph of hematoxylin and eosin stained, 5 µm thick paraffin embedded tissue section illustrating the histology surrounding the ring electrode cavity (*) with subcutaneous tissue (i), subgaleal tissue (ii), the skull (iii), and arrow indicating high magnification section in inset C. Inset C (scale bar = 200µm) shows the fibrotic area (dashed line) and how the distance (dashed arrow) was measured. The length of fibrosis extending laterally from the electrode cavity along the subgaleal cleavage plane was variable. This was due to different levels of blunt dissection tool application during implantation. The fibrotic tissue filling of the cleavage had minimal number of inflammatory cells (high magnification inset D, scale bar = 50µm). The skull and periosteum were unremarkable. Minimal fibrous scarring beside the implant is along the plane of surgical dissection. Figure 6 is showing a better result (less fibrotic tissue) as a tunneling tool (cannula) was used more extensively.

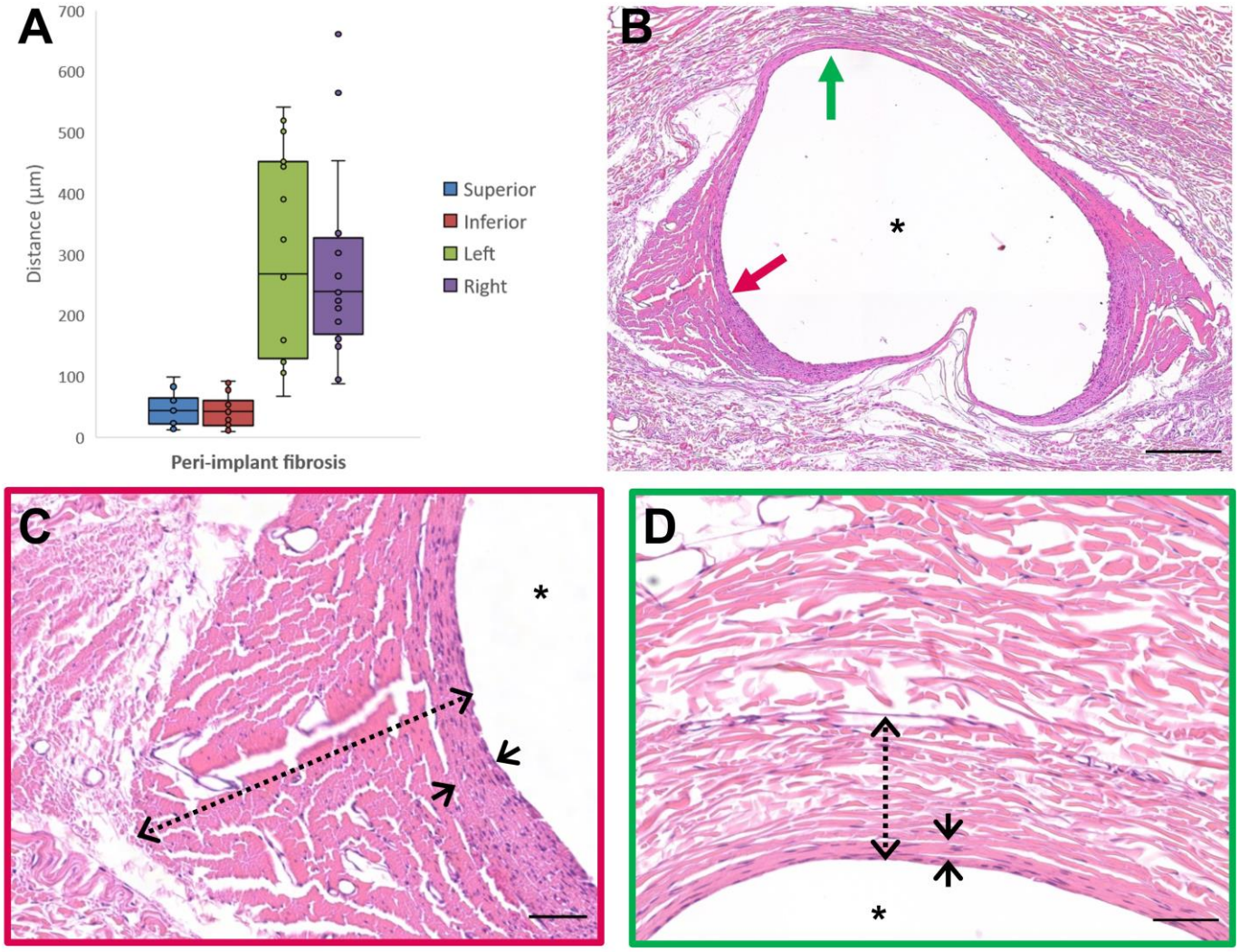

Figure 8 Peri-implant fibrosis. A shows fibrotic thickness measured on all sides of the implant cavity for S3-7. B-D are photomicrographs of hematoxylin and eosin stained, 5 µm thick paraffin embedded tissue section illustrating the histology surrounding one ring electrode cavity (*). Inset B (scale bar = 200µm) shows whole electrode cavity (1.2mm, the non-round shape is a processing artifact) with arrows indicating high magnification sections in insets C and D (scale bar = 50µm) that show peri-implant fibrosis (dashed arrow, and thickness of fibrotic encapsulation (open arrows) on the left and superior side of the cavity. Fibrotic sections are partially lined with uni and multi-nucleated histiocytes. Minimal fibrous scarring beside the implant is along the plane of surgical dissection.

Subject	Electrode	Histiocytic Response	Chronic Inflammation	Acute Inflammation
S03	2	1	0	0
S03	3	1	1	1
S03	4	1	1	1
S04	1	1	0	0
S04	2	2	1	0
S04	2*	1	0	0
S04	3	1	0	0
S04	4	3	1	1
S05	1	1	1	0
S05	2	1	1	0
S05	3	0	0	0
S05	4	1	0	1
S06	1	3	1	1
S06	1*	1	1	1
S06	2	2	1	1
S06	3	1	1	0
S06	4	1	1	1
S07	1	3	2	2
S07	2	2	2	2
S07	3	1	0	0
S07	4	1	1	0

Table 1 Qualitative histopathology assessment for S3-7 with * indicating another sample from the same electrode. Chronic and acute inflammation was minimal except for channel 1 in S07. There was variation in histiocytic response within and across subjects. This variability may relate to differences in implantation. Acute inflammatory response caused by infection. Histiocytic response was ranked 0- not present, 1- single layered, 2- multi-layered, 3- multi-layered with multi-nucleated giant cells. Chronic (mononuclear) and acute inflammatory response were ranked 0 to 3 with 3 indicating higher level of response. S01-2 were not included as they were used for the histopathological method development. Overall, percent of ranks 0, 1, 2, and 3 were 31%, 53%, 11%, and 5% respectively.

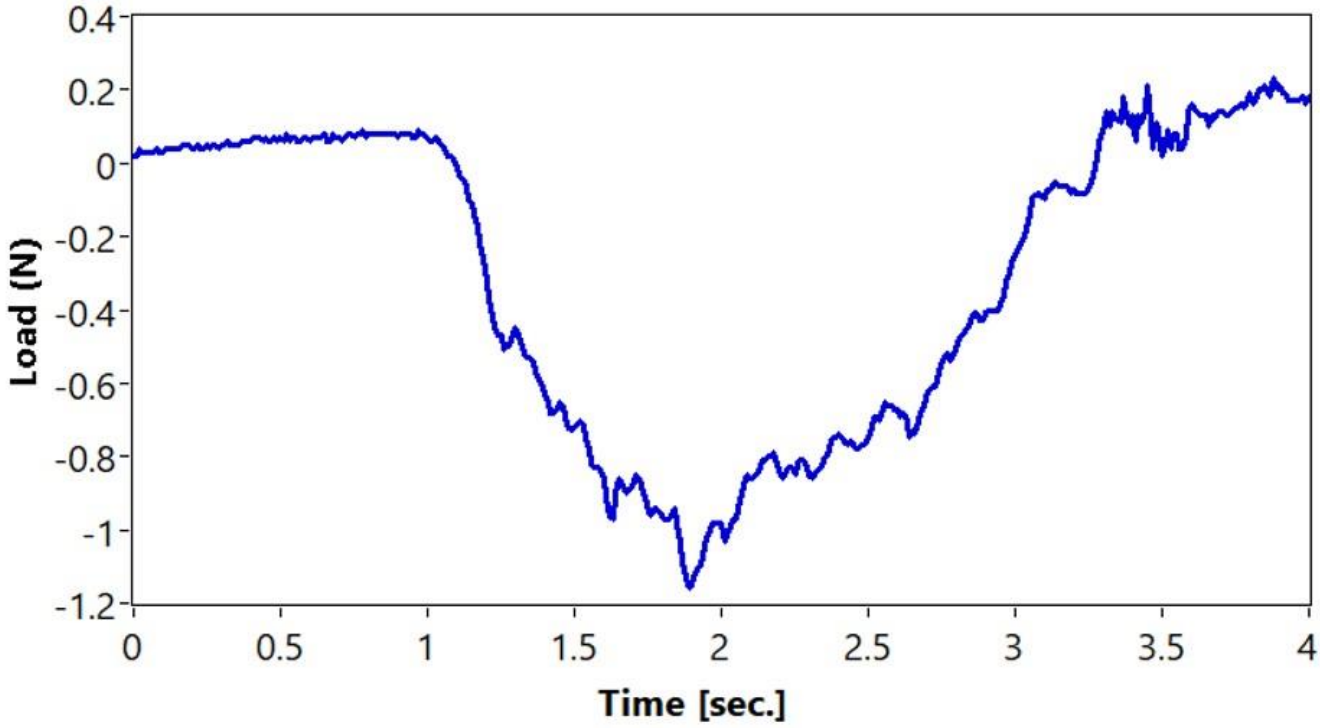

Figure 9 Representative example of passive array implanted along the dorsal flank, extraction force over about 3 seconds of steady pull. The maximum force was 1.16N and the array remained intact.

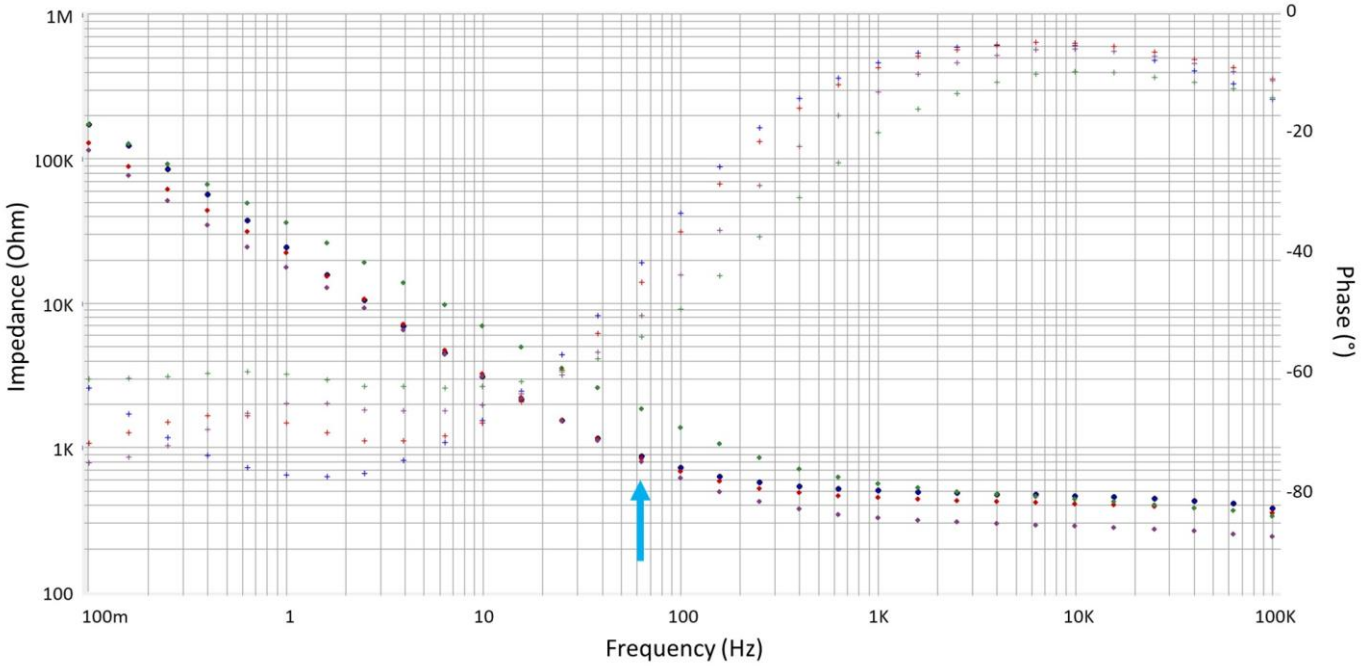

Figure 10 Representative example of impedance spectroscopy. Blue, red, purple, and green data points indicate impedance (◊) and phase (+) for E1, E2, E3, and E4 respectively. Measurements were made with adjacent electrode as reference and the other channel (2 electrodes) as counter. Impedance measurements were comparable to the active recording electrodes on the head at 62.5Hz (frequency used to do the continues impedance measurements, blue arrow).

Highlights

- Long-term, stable EEG recordings are required for diagnosis and management of epilepsy.
- Ring electrodes provide stable EEG, reasonably low artifact, and mechanical stability.
- Ring electrodes are minimally-invasive, simple to insert, and can be removed without breakage.
- Tissue response after 3-5 months of implantation is minimal.
- Signal quality measures were stable over the implantation period.

Novelty & Significance

This article describes the usefulness of a novel sub-scalp electrode array inserted between the periosteum and subgaleal plane and recording from both hemispheres of the brain. The study was conducted for several months and provides insights into long-time use of this device. This is significant as electrode placement safety, minimal fibrotic response, and long-term stability of recordings is necessary for regulatory approvals. This minimally invasive device is advantageous for diagnosis and management of neurological conditions such as epilepsy, stroke, and sleep where long-term, EEG monitoring is beneficial.

Graphical abstract

Preclinical safety study of a fully implantable, sub-scalp ring electrode array for long-term EEG recordings

Minimally invasive, biocompatible implant recorded stable EEG up to 5 months with minimal tissue response.
This is useful for diagnosis and management of neurological conditions where long-term, EEG monitoring is required.

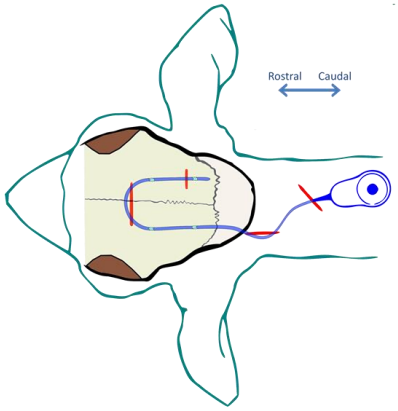

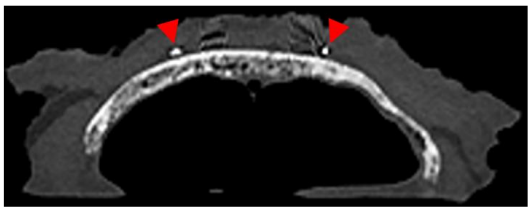

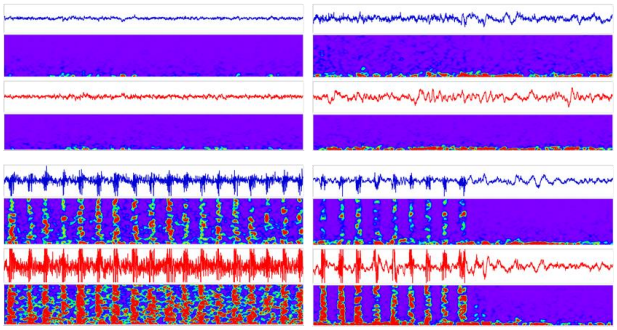

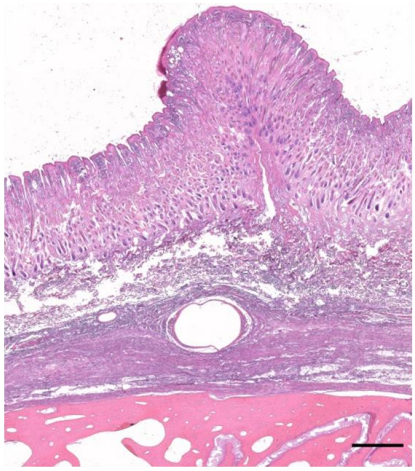

Bionics institute

THE UNIVERSITY OF MELBOURNE